High-frequency response of the ocean to mountain gap winds in the northeastern tropical Pacific

Jun-Hong Liang,[1] James C. McWilliams,[1,2] and Nicolas Gruber[1,2,3]

Received 6 March 2009; revised 18 August 2009; accepted 25 August 2009; published 2 December 2009.

[1] The wind jets generated by the three mountain gaps of Central America have a substantial impact on the mean state of the northeastern tropical Pacific. Here, we study the mean oceanic impact of individual high-frequency wind events by synthesizing satellite and reanalysis products. Using daily sea level wind and sea level pressure (SLP) for the period from 1999 through 2007, we identified a total of 103 short-term wind events for the Gulf of Tehuantepec, 59 events for the Gulf of Papagayo, and 36 events for the Gulf of Panama, most of them occurring between November and May. On the day of maximum wind, the composite peak wind speed reaches about 15 cm/s across nearly the entire Gulf of Tehuantepec, while the winds in the other two gulfs are somewhat weaker. Downwind of the gaps, the composite mean sea surface temperature (SST) drops substantially within one day in response to these wind events, but the spatial extent of the changes remains limited to the region of high wind speed. The high correlation with wind speed suggests that the cooling is mainly a response to wind-driven turbulent mixing rather than wind stress curl induced upwelling. The boundary layer turbulence is strongly shear-driven and weakly convectively driven in the Gulf of Tehuantepec and purely shear driven in the other two gulfs. Mean SST recovers quickly after the event, with the recovery largely being controlled by the anomalous surface heat flux induced by the SST disturbance. Each wind event is followed by a phytoplankton bloom, as evidenced by strong increases in satellite detected chlorophyll-*a* (Chl-*a*) and inferred net primary production (NPP). The initial response of chlorophyll and NPP is delayed relative to SST by only one day, likely owing to upward mixing of chlorophyll from the deep chlorophyll maximum. Chlorophyll remains elevated for several days after the SST has already recovered suggesting that the upward mixing of new nutrients has sustained the bloom. This is supported by the observation that the chlorophyll response remains also limited to the region of high wind speed. These wind events contribute substantially to the overall NPP in the northeastern tropical Pacific. In contrast to SST and Chl-*a*, the response of sea surface height (SSH) to these wind events appears to involve both local coastal recirculations and regional mesoscale activities.

Citation: Liang, J.-H., J. C. McWilliams, and N. Gruber (2009), High-frequency response of the ocean to mountain gap winds in the northeastern tropical Pacific, *J. Geophys. Res.*, *114*, C12005, doi:10.1029/2009JC005370.

1. Introduction

[2] There are three narrow mountain gaps in the Central America cordillera, (i.e., the Chivela Pass next to the Gulf of Tehuantepec in Mexico; the Lake of Nicaragua and the lowlands around the lake next to the Gulf of Papagayo; and the Central Isthmus of Panama next to the Gulf of Panama), where the elevations are more than 2000 meters lower than their surroundings (Figure 1). The existence of mountain wind jets has been recognized for a long time [*Frankenfield*, 1917; *Hurd*, 1929] due to their importance for local climate, fishery, and navigation, but only the advent of satellite observations has permitted a full description of their origins and structures [*Chelton et al.*, 2000a].

[3] Wind jets over the Gulf of Tehuantepec are mainly caused by cold surge outbreaks from the North American continent. Wind jets over the Gulfs of Papagayo and Panama can be due to either cold surges or easterly trade wind bursts blowing over the Caribbean Sea. After funneling through the mountain gaps, the jets fan out while extending a few hundred kilometers into the Pacific. Jets over the Gulfs of Tehuantepec and Panama turn anticyclonically after leaving the coast because of the adjustment of the inertial balance at the gaps to the geostrophic balance over the open ocean [*Clarke*, 1988; *Steenburgh et al.*, 1998; *Chelton et al.*, 2000b]. Jets over the Gulf of Papagayo

[1]Department of Atmospheric and Oceanic Sciences, University of California, Los Angeles, California, USA.
[2]Institute of Geophysical and Planetary Physics, University of California, Los Angeles, California, USA.
[3]Institute of Biogeochemistry and Pollutant Dynamics, ETH Zurich, Zurich, Switzerland.

0148-0227/09/2009JC005370$09.00

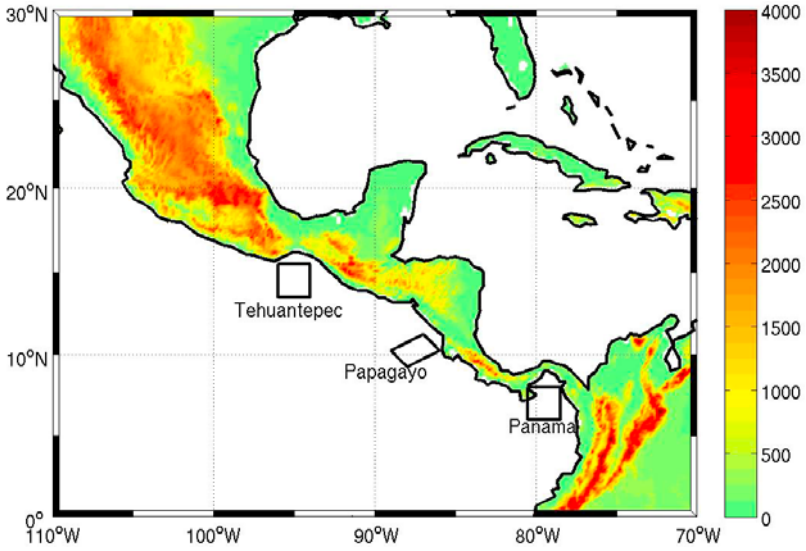

Figure 1. The orography of the Central America region. Black boxes indicate three nearshore regions in the Gulfs of Tehuantepec, Papagayo, and Panama that were used to compute the average indices.

continue southwestward after leaving the coast, indicating the wind is already in near-geostrophic balance at the mountain gap. This has been ascribed to the fact that the effective width of the Papagayo gap is wide [*Chelton et al.*, 2000b]. The jets fan off their axis after leaving the mountain gaps because of a strong cross-flow pressure gradient away from the jet axis [*Steenburgh et al.*, 1998].

[4] Strong wind jets blowing over the ocean induce unique oceanic responses. The low-frequency response of the ocean to climatological gap outflows has been investigated thoroughly. Regional circulations [*Kessler*, 2006; *Rodríguez-Rubio et al.*, 2003] and subsurface thermal structures [*Xie et al.*, 2005; *Kessler*, 2006] are highly influenced by climatological gap wind outflows as revealed by satellite and in situ observations. *Sun and Yu* [2006], based on a regional ocean modeling study, found that the mechanical forcing of low-frequency gap outflows strongly modulate the annual variation of sea surface temperature (SST) in the Gulfs of Tehuantepec and Papagayo. Using satellite images, *McClain et al.* [2002] suggested that wind-induced upwelling is responsible for the high chlorophyll-*a* (Chl-*a*) that is observed downwind of the three mountain gaps.

[5] In contrast to the low-frequency response, the oceanic response to high-frequency gap wind events has been studied only for a couple of individual events [*Barton et al.*, 1993; *Trasviña et al.*, 1995; *Trasviña and Barton*, 2008] or using idealized numerical simulations [*McCreary et al.*, 1989]. Based on an in situ survey in the Gulf of Tehuantepec and satellite images, *Trasviña et al.* [1995] found that asymmetric circulations spun up during the wind event with a much stronger anticyclonic eddy at the right flank of the wind track. They also concluded that the dramatic decrease of SST during the wind event is due largely to wind-generated turbulent entrainment instead of enhanced latent heat flux. *Trasviña and Barton* [2008] found that a dipole consistent with linear Ekman theory [*Crepon and Richez*, 1982] spun up after a summer wind event in the Gulf of Tehuantepec and the cyclone dissipated in a few weeks. *McCreary et al.* [1989] forced a 1.5 layer model with wind events that are similar to typical Tehuantepec and Papagayo wind events and concluded that the preferential generation of anticyclonic eddies is due to the shallowness of the local thermocline, which inhibits strong Ekman suction associated with cyclonic eddies.

[6] Utilizing satellite and reanalysis data products spanning 8 years, this study seeks to characterize the oceanic responses to typical high-frequency gap wind events by the statistical compositing of all identified events at each of the three gap sites. We aim to understand the physical processes and biological consequences of the oceanic responses, and to show the connection between the high-frequency gap wind events and regional mesoscale activities. Relative to prior studies, our investigation is based on the statistical average of a large number of events across multiple years and all Gulfs, permitting us to extract the typical behavior in all three regions. Section 2 introduces the data sets and the identification of the high-frequency gap wind events, while Section 3 describes the characteristics of the identified events. In section 4, we discuss the cooling of the sea surface due to the wind events and how SST recovers afterwards. Section 5 examines the Chl-*a* response and its implication for net primary production. Section 6 discusses the possible connection between wind events and regional mesoscale variability. The section 7 summarizes this study and puts our results into the context of other mountain gap winds.

2. Data Description

[7] Daily ocean surface wind data on a 0.25° × 0.25° grid from July 1999 to June 2007 were taken from the level 3 daily, gridded 10 meter vector wind product (http://podaac.jpl.nasa.gov) based on data retrieved by the SeaWinds scatterometer on the QuikSCAT satellite. The SeaWinds scatterometer wind retrievals are accurate to better than 2 m/s in speed and 20° in direction, which is comparable to in situ point measurements from buoys [*Chelton et al.*, 2004].

[8] Weekly sea surface height (SSH) anomaly data on a $1/3^\circ \times 1/3^\circ$ grid from July 1999 to June 2007 were obtained from the Ssalto/Duacs multimission altimeter gridded sea-level anomaly product (http://www.aviso.oceanobs.com/en/data/product-information/duacs/index.html), which merge data from up to four satellites. *Pascual et al.* [2006] show that the multisatellite altimeter product resolves more ocean mesoscale variability than previous altimeter products.

[9] Daily SST between July 1999 and June 2007 on a $0.25^\circ \times 0.25^\circ$ grid comes from the Tropical Rainfall Measuring Mission Microwave Imager (TMI) SST product (http://www.ssmi.com). Microwave SST retrieval can be performed in almost all weather conditions except during rain. This is a big advantage compared to an infrared-based SST retrieval that fails in cloudy and rainy weather and degrades in the presence of atmospheric aerosols [*Wentz et al.*, 2000].

[10] Daily Chl-*a* concentration and photosynthetic active radiation (PAR) on a $0.083^\circ \times 0.083^\circ$ grid from July 1999 to June 2007 come from the data gathered by the Sea-viewing Wide Field-of-view Sensor (SeaWiFS) (http://daac.gsfc.nasa.gov), which measures ocean colors using eight spectral bands of water-leaving radiance in visible and infrared wavelengths in clear sky. There is a large amount of missing data near the coast of South America and the Intertropical Convergence Zone (ITCZ) due to cloud cover. The Chl-*a* and PAR data are interpolated onto the grid of the TMI SST product for the calculation of net primary production (NPP). The latter is based on the Vertically Generalized Production Model (VGPM) algorithm [*Behrenfeld and Falkowski*, 1997], which relates NPP to surface Chl-*a* concentration, PAR and SST.

[11] In addition to satellite data, three reanalysis products are used. Sea level pressure (SLP) on a $2.5^\circ \times 2.5^\circ$ grid between July 1999 and June 2007 comes from the National Centers for Environmental Prediction-Department of Energy (NCEP-DOE) reanalysis product [*Kanamitsu et al.*, 2002]. Ocean surface radiation flux between July 1999 and December 2006 comes from the International Satellite Cloud Climatology Project (ISCCP) [*Rossow and Schiffer*, 1991]. The noontime surface radiation on a 2.5×2.5 grid is used when estimating sea surface warming. The net ocean-atmosphere heat flux between July 1999 and December 2004 was obtained from ftp://ftp.whoi.edu/pub/science/oaflux/data_v3/daily/netheat_1985–2004. The product combines ISCCP ocean surface radiation fluxes and the Objectively Analyzed Air-Sea Fluxes (OAFlux) turbulent air-sea flux product [*Yu and Weller*, 2007].

[12] The high-frequency anomaly data used in this study were obtained as follows: For each grid point, a temporal mean and a smoothed seasonal cycle were first removed to obtain a nonseasonal anomaly. After that, a high-pass filter was applied to essentially remove the variabilities with periods longer than 90 days, such as El Niño and Southern Oscillation (ENSO) events that are present in both gap wind [*Romero-Centeno et al.*, 2003] and oceanic responses [*Palacios and Bograd*, 2005]. For surface Chl-*a* concentration, the aforementioned operations were performed after applying a natural logarithmic transformation to the data since oceanic Chl-*a* concentration approximately follows a lognormal distribution [*Campbell*, 1995].

[13] The high-frequency wind events were identified based on a wind and a pressure index, constructed from high-frequency anomalous wind vectors and SLP. The wind index was defined for each gap region using the offshore component of the high-frequency wind velocity vector anomaly in the nearshore regions shown in Figure 1. These regions were chosen to capture the narrow wind jets and to have sufficient data points to reduce sampling error. The pressure index was defined on the basis of the high-frequency SLP anomaly difference across the mountain gaps. With these two indices, a wind event was identified if all of the following criteria were met: 1) the wind index exceeds a threshold of 1.5 standard deviations above the mean of the full time series of the wind index; 2) the average wind indices from day -7 to day -3 before a wind event and from day 3 to day 7 after a event are less than one half standard deviations above the mean of the full time series of the wind index; 3) the offshore wind is strongest within ± 7 days of the event days; 4) the pressure index on day -1 and day 0 exceeds a threshold of 1 standard deviation above the mean of the full time series of the pressure index. This set of criteria finds strong and transient wind events that are forced by substantial cross-gap pressure differences.

[14] All events for each region were then composited into an average response, using the day at which the wind index reaches its maximum as day 0. Missing data were filled by the average of the data on the two neighboring days at the same grid point if they are both available and were ignored otherwise. The statistical significance was assessed using a student's *t* test.

3. High-Frequency Gap Wind Events

[15] Between July 1999 and June 2007, 103 Tehuantepec wind events, 59 Papagayo wind events, and 36 Panama wind events were identified. This is a minimum estimate, since some wind events might have been missed because of rain contamination and the nondaily coverage of QuikSCAT. The identified wind events exhibit a strong seasonal variability. All Panama events, and most Tehuantepec and Papagayo events occur between November and May. This conforms to the seasonal variability of the cold surge outbreaks that force most wind events in the Gulf of Tehuantepec, and some of those in the Gulfs of Papagayo and Panama. The other Papagayo and Panama events are the results of the high-frequency variability of the easterly trade wind over the Caribbean Sea (the Caribbean Low-Level Jet), which also achieves its maximum strength in winter [*Wang*, 2007]. Tehuantepec wind events between June and September are due to episodic low-pressure systems residing in the eastern Pacific warm pool (L. Bosart, personal communication, 2008). Papagayo events between June and September are attributed to the high-frequency variability of the trade wind albeit its strength in summer is weaker than in winter.

[16] The composite time series of the wind index during wind events in the three gulfs are shown in Figures 2a, 2c, and 2e. In the Gulf of Tehuantepec, the offshore wind anomaly reaches its maximum strength of about 11 m/s on the day of the event. Considering the climatological wind speed of 4 m/s, the absolute wind speed during the peak of

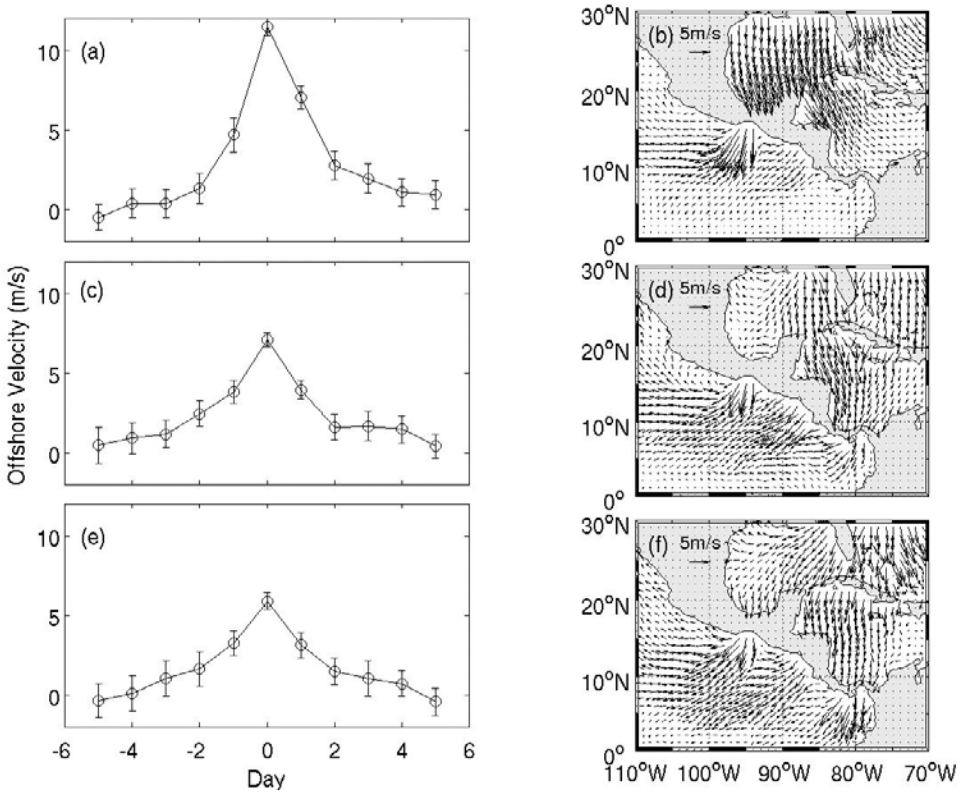

Figure 2. Composite offshore wind speed anomalies (m/s) for (a) Tehuantepec wind, (c) Papagayo wind, and (e) Panama wind. Composite maps of wind vector anomalies on day 0 for (b) Tehuantepec wind, (d) Papagayo wind, and (f) Panama wind. Error bars indicate 5–95% confidence range. Day 0 corresponds to the day when offshore wind is strongest.

an average event amounts to about 15 m/s. In the gulfs of Papagayo and Panama, the offshore wind anomalies are significantly weaker, reaching a maximum of about 6 m/s. Considering the climatological winds of about 3 m/s, the absolute wind speeds are about 9.5 m/s, substantially above the mean ocean wind speed in the northeastern tropical Pacific of about 4.5 m/s. In all regions, the wind events are short (on average about 4 days) and intensify and weaken very rapidly. The time series of the pressure index (not shown) are similar to those of the wind index for the three gap winds.

[17] Figures 2b, 2d, and 2f show the composite maps of high-frequency velocity anomaly at the peak time of the wind events. After leaving the mountain gaps, the Tehuantepec and Panama winds turn anticyclonically, while there is no significant change of direction in the Papagayo wind. These findings are in agreement with the already discussed results of *Chelton et al.* [2000b], who showed on the basis of the NSCAT winds that the wind direction changes in the Gulfs of Tehuantepec and Panama are the result of an adjustment from an inertial balance at the mountain gap to a geostrophic balance over the open ocean. Since the Panama wind is weaker and the region is located closer to the equator with a smaller Coriolis parameter, the change of direction is not as large as observed for the Tehuantepec wind. For the Papagayo wind, the lack of a directional change is interpreted to be the result of it being already in near-geostrophic balance at the wide mountain gap [*Chelton et al.*, 2000b]. The spatial extent over which the impact of the mountain gap winds over the ocean can be discerned is large. The areas, over which the composite wind speed is more than 5 m/s above normal on day 0 are approximately 2×10^5 km^2 for all three gap wind regions. There is no statistically significant difference in the composite time series and the composite wind vector maps for wind events forced by the two different mechanisms, i.e., the cold surge outbreak and the high-frequency variability of the Caribbean Low-Level Jet, in both the Gulf of Papagayo and the Gulf of Panama (not shown).

4. SST Response

4.1. Sea Surface Cooling

[18] The northeastern tropical Pacific has a relatively warm SST and a relatively shallow surface mixed layer due to the comparatively weak wind and strong sea surface heating over this region. Previous studies [e.g., *Trasviña et al.*, 1995] have shown that individual wind events can trigger strong cooling of the sea surface. To quantify the magnitude of the sea surface cooling due to gap wind outbreaks, SST indices in the three gulfs were defined by averaging the high-frequency SST anomaly over the nearshore domains in the three gulfs indicated in Figure 1. These are regions where the winds are strongest.

[19] Figures 3a, 3c, and 3e (black lines) show the composite time series of the nearshore SST indices from 5 days before the day of the maximum wind speed to 15 days afterwards. The SST anomalies start to decrease immediately when the offshore wind strengthens two days before the day

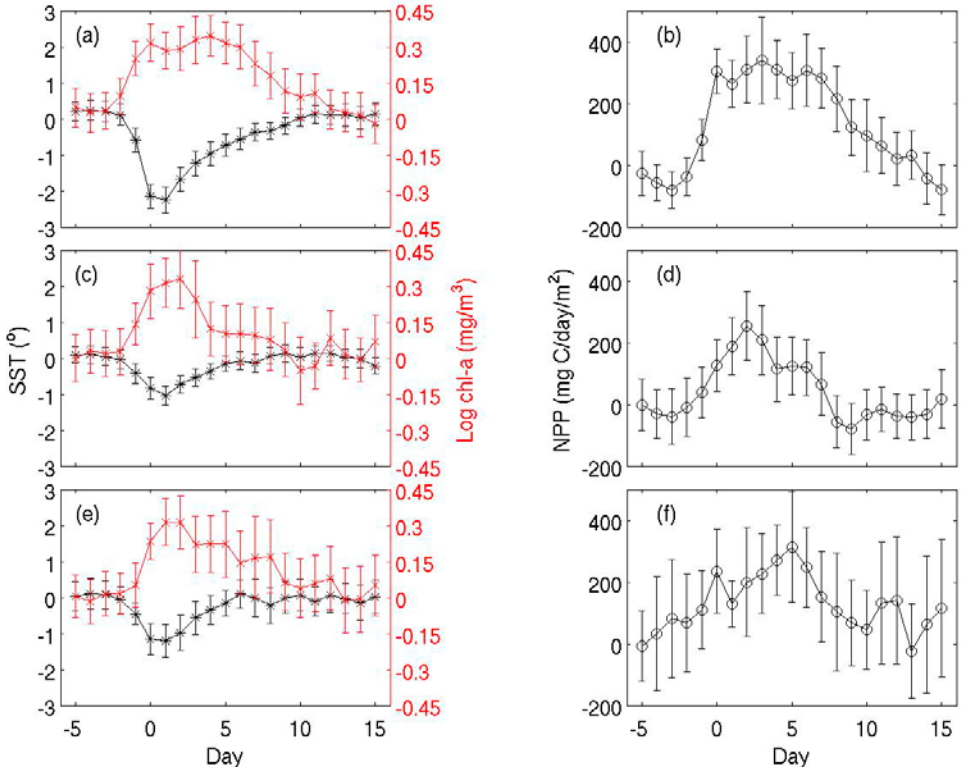

Figure 3. Composite time series of high-frequency SST anomaly (black lines) and high-frequency natural logarithmic chlorophyll-*a* concentration anomaly (red lines) for (a) Tehuantepec wind, (c) Papagayo wind, and (e) Panama wind. Composite time series of high-frequency NPP for (b) Tehuatepec wind, (d) Papagayo wind, and (f) Panama wind. Error bars indicate 5–95% confidence range. Day 0 corresponds to the day when offshore wind is strongest.

of maximum wind. The decrease is most dramatic between day −1 and day 0 when the wind intensifies most significantly. The nearly instantaneous response of SST to the wind changes suggests that the cooling is due to boundary layer turbulent mixing that entrains subsurface cold water to the surface mixed layer. This is consistent with previous observational results for individual events in the Gulf of Tehuantepec [*Trasviña et al.*, 1995], which were based on observations across the upper ocean, and not just on the thin surface layer that satellites observe. Using measurements of shear, stratification, and both static and dynamic stability, these authors showed that surface cooling results primarily from mixing. Thus, the few in situ event observations from the Gulf of Tehuantepec appear to have captured the mean response across all Gulfs. SST continues to cool after the day of maximum wind, with the minimum SST reached on day 1. The largest negative SST anomalies are more than 2°C in the Gulf of Tehuantepec, and larger than 1°C in the Gulfs of Papagayo and Panama, respectively. The SST anomaly starts to increase after day 1 with the recovery taking a few days. The sea surface warming process will be discussed in the next subsection.

[20] Figure 4 shows the composite maps of the high-frequency SST anomaly passing the 95% student *t* significance test on day 1 when nearshore SST anomalies are largest. In all three places, the negative SST anomalies fill the whole gulfs and extend from the coast well into the open ocean along the wind tracks. The maximum sea surface cooling occurs just offshore of the mountain gaps. The distribution of the SST signals is spatially very congruent with the wind tracks. The negative SST anomaly turns to the west outside of the Gulfs of Tehuantepec and Panama, while the negative SST anomaly goes southwest after leaving the coast of Costa Rica. The congruence of the dominant SST signals and the wind tracks adds further support to our previous conclusion that turbulent mixing instead of upwelling causes the sea surface cooling observed in the days around the day of maximum wind speed, since wind curl induced upwelling would lower SST at the left flank of the wind track and increase SST at the right flank of the wind track, neither of which is observed in the first few days of the events. Wind curl induced upwelling and downwelling does occur later, typically within a week after wind event, as can be inferred from SSH map that will be shown in Section 6 and from individual SST maps. However, their composite SST signals are not statistically significant (not shown).

[21] There are two mechanisms that can generate strong boundary layer turbulence under strong wind: shear turbulence and surface cooling induced convective turbulence. Shear turbulence is the result of a strong wind-driving surface-intensified current that induces strong horizontal and vertical shear. Convective turbulence is the result of wind induced evaporation and latent heat fluxes that make the surface waters convectively unstable. In the Gulf of Tehuantepec, the enhanced heat loss is so strong that the composite net heat flux, estimated on the basis of reanalysis data, changes from around 50 W/m^2 heating before wind events to around 185 W/m^2 cooling on the

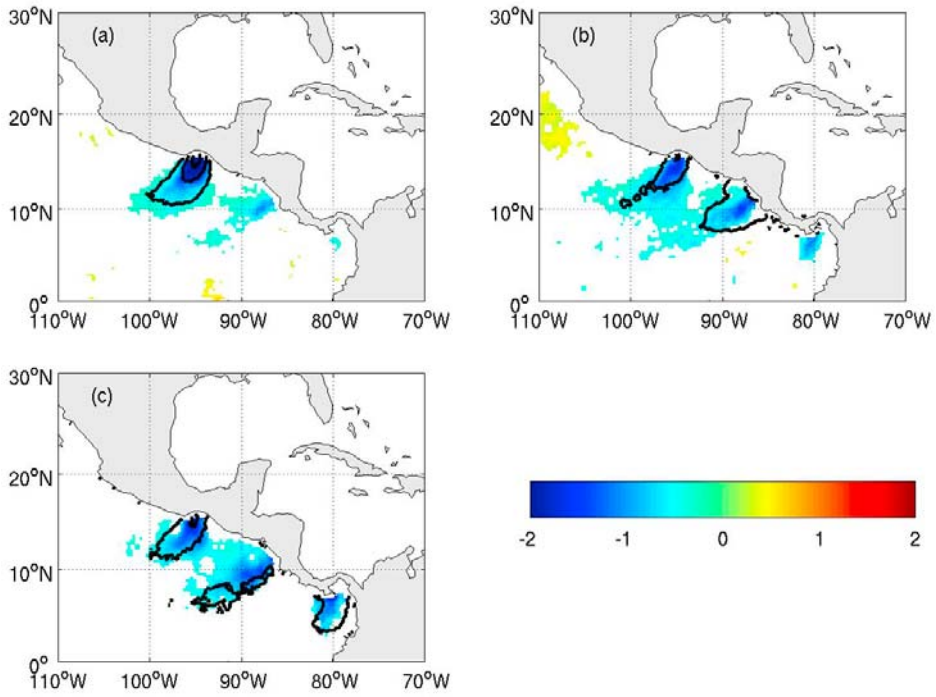

Figure 4. Composite maps of the high-frequency SST anomaly (°C) passing 95% student *t* significance test on day 1 for (a) Tehuantepec wind, (b) Papagayo wind, and (c) Panama wind. (Contours indicate wind speed of 4, 8, and 12 m/s.)

day of maximum wind, i.e., making the surface boundary layer change from stable to unstable. In the Gulfs of Papagayo and Panama, the wind jets are weaker and the incoming solar fluxes are stronger. The net heat fluxes are still positive on the days of maximum winds, although significantly reduced. As a result, the oceanic boundary layer remains thermally stable.

[22] To understand the importance of convective turbulence and shear turbulence during Tehuantepec wind events, the Monin-Obukhov length (h_{MO}) was estimated from the composite wind stress and the net heat fluxes as $h_{MO} = \rho C_p(\tau/\rho)^{3/2}/(\kappa\alpha g Q_{net})$ where ρ, C_p, and α are the density, specific heat, and thermal expansion coefficient of sea water, respectively; κ is the von Karman constant; g is gravity; τ is the wind stress; and Q_{net} is the net heat flux from the atmosphere to the ocean. The Monin-Obukhov length on Tehuantepec event day is approximately -300 m. The typical mixed layer depth ($h_{ml} > 0$) in the Gulf of Tehuantepec is typically a few tens of meters, i.e., $0 > h_{ml}/h_{MO} \gg -2$. This indicates that the turbulence in the oceanic boundary layer is weakly convectively driven and strongly shear driven under Tehuantepec wind jets, and is purely shear driven under Papagayo and Panama wind jets. *Trasviña et al.* [1995] also reached the same conclusion that shear turbulence is much more important in deepening the mixed layer on the day of maximum wind in the Gulf of Tehuantepec, however, their estimation was based on conductive heat transfer.

4.2. SST Recovery

[23] After SST reaches its minimum on day 1, it recovers to its preevent value in a few days. This fast recovery can be the result of three mechanisms: a positive horizontal eddy heat flux, a positive horizontal heat flux due to subduction, and a positive surface heat flux anomaly. The first mechanism is associated with the recirculations that spin up on both flanks of the wind tracks after each wind event [*Trasviña et al.*, 1995; *Barton et al.*, 2009]. These recirculations provide an eddy-driven net positive heat flux towards the cool sea surface under the wind tracks. The second mechanism is associated with the subduction at frontal regions [*Trasviña et al.*, 2003a]. The third mechanism can be important when near-surface atmospheric temperature remain largely unaffected by the wind events. In such cases, a negative SST anomaly of $-\delta T$ implies an anomaly of δT in air-sea temperature difference, leading to a positive heat flux anomaly (δQ) from the atmosphere to the ocean. To first order approximation, $\delta Q = \lambda \cdot \delta T$, where λ is a scaling factor that increases equatorward and when the scale of the SST disturbance decreases [*Bretherton*, 1982].

[24] In order to assess the feasibility of the third mechanism, we attempt to estimate the e-folding time scale of the SST recovery (Γ), and compare it to the observed e-folding time scales, which are 4.8 days, 4.5 days, and 3.1 days for the Gulfs of Tehuantepec, Papagayo and Panama, respectively. These values were diagnosed by a least squares regression on the composite time series of the SST indices in the three gulfs, respectively.

[25] *Price et al.* [2008] show that the e-folding time scale of the SST recovery (Γ) is inversely proportional to the surface heat flux anomaly, and directly proportional to the surface wind stress τ, i.e.,

$$\Gamma = c\frac{\tau}{\lambda \cdot \sqrt{Q_n}}, \tag{1}$$

where τ has a unit of [Nm^{-2}]; Q_n is the noontime heat flux [$Wm^{-2}=Nm^{-1}s^{-1}$]; and where $c=2.7\times10^{10}N^{1/2}m^{1/2}s^{-1/2}C^{-1}$ is a constant. The parameter λ describes how the heat flux changes for a given change in SST, and was shown to depend on the size of the region with anomalous SSTs [*Bretherton*, 1982]. This author noted that the value of λ is around 100 W/(m^2°C) for SST disturbance extending over some tens of kilometers. The nearshore domains in the three gulfs are about 200 kilometers across, permitting us to assume that Bretherton's value is still applicable, i.e., we chose a λ of 100 W/(m^2°C). A more detailed estimation of the parameter λ would require numerical experiments using atmospheric general circulation models and, therefore, is beyond the scope of this study. With these assumptions, we diagnose from equation (1) the values of Γ of 4.5 days, 3.9 days, and 4.3 days, in the three gulfs respectively, very close to the observed recovery time scales. This close agreement between the observed and the modeled time scales suggests that the positive surface heat flux anomaly associated with the negative SST disturbance is very important in the fast sea surface warming after wind events.

[26] In order to check this conclusion, we next evaluate also the trapping depth D, i.e., the depth to which a heat flux anomaly maximally penetrates. It reflects the competition of the deepening effect of the wind-driven turbulent mixing and the stratification effect due to the positive surface heat flux anomaly. The trapping depth can be computed from [*Price et al.*, 1986, 2008]

$$D = C_D \frac{\tau/\rho}{\sqrt{Q_*/P_Q}}, \tag{2}$$

where C_D = 1.2 is the similarity constant [*Price et al.*, 2008]; P_Q is half the duration of positive heat flux (roughly 6 hours); and Q_* is the noon time buoyancy flux ($Q_* = Q_n g\alpha/(\rho^2 C_p)$ with gravity g, density ρ, heat capacity C_p, and thermal expansion coefficient α).

[27] After wind events, the ocean surface wind speeds from the QuikSCAT wind vector product are 5.2 m/s, 4.5 m/s and 4.8 m/s in the three gulfs, respectively; and the noontime surface heat fluxes base on the ISCCP radiation flux product and the OAFlux latent and sensible heat flux product are 605 W/m^2, 652 W/m^2, and 532 W/m^2 in the three gulfs, respectively. Using equation (2), the trapping depths (D) corresponding to the aforementioned weather conditions are 9.6 m, 7.1 m, and 8.7 m in the three gulfs, respectively. Thus, the positive heat flux anomalies are trapped within a thin layer of less than 10 meters as a result of relatively weak wind and strong heat flux. The shallow trapping depth is favorable for the quick sea surface warming, supporting our conclusion that surface warming is very important in the rapid SST recovery after the wind event.

5. Biological Response

[28] Chlorophyll-*a* is the primary photosynthetic pigment in phytoplankton and is a good indicator of phytoplankton biomass. Phytoplankton biomass in the northeastern tropical Pacific outside the gap wind areas tend to be relatively low, mainly owing to the highly stratified conditions characterizing this part of the Pacific, preventing the limiting nutrients to reach the euphotic zone. In contrast, phytoplankton is strongly enhanced, on average, downwind of the gap areas, likely because of the wind jets enhancing the upward nutrient transport [*McClain et al.*, 2002]. What has not been established yet is the contribution of individual wind events to the enhanced chlorophyll levels, a gap that we would like to address next. In the previous section, we have seen that vertical mixing is greatly enhanced when the strong wind blows. We will show in subsequent paragraphs that biological processes also change under the strong wind and all these changes are reflected in the observed ocean surface Chl-*a*. To quantitatively characterize physical and biological activities during and after high-frequency wind events, Chl-*a* indices in the three gulfs are defined by taking the average of the natural logarithmic Chl-*a* concentration anomaly in the nearshore regions indicated in Figure 1.

[29] Figures 3a–3c (red lines) display the composite time series of the Chl-*a* indices from 5 days before the day of maximum wind to 15 days afterwards. Similar to the initial SST response, Chl-*a* responds very quickly to the onset of the wind, with the initial Chl-*a* increase starting two days before the day of maximum wind. This nearly instantaneous response is surprising, as phytoplankton response to wind events often tend to be delayed by several days, a result of the phytoplankton community requiring time to take advantage of the new nutrients. We suspect that this fast response is due to vertical mixing, analogous to the SST response. In this oceanic region, Chl-*a* tends to increase with depth until the deep chlorophyll maximum (DCM), and decreases with depth beyond the DCM. The annual mean DCM is typically a few tens of meters in the three gulfs according to the World Ocean Atlas 2001 (WOA01) [*Conkright et al.*, 2002]. As a consequence, surface Chl-*a* will increase when turbulent mixing entrains subsurface water of higher Chl-*a* around the DCM to the ocean surface. After a first peak on day 0, the Chl-*a* index for Tehuantepec dips slightly and then continues to increase until a maximum is reached on day 5. This second phase of increase is likely the result of the new growth of phytoplankton owing to the injection of the limiting new nutrients. The relatively fast recovery of SST could support the phytoplankton growth, as it enhances stratification and hence the average availability of light. On the other hand, loss processes, such as zooplankton grazing and horizontal and vertical export may prevent near surface biomass to increase to even larger levels. After day 6, surface Chl-*a* decreases gradually. At that time, the extra nutrients entrained by vertical mixing may have been consumed and zooplankton grazing and export starts to dominate over phytoplankton growth. The composite time series of high-frequency Chl-*a* concentration anomaly are similar for the Papagayo and Panama winds, although the day of maximum chlorophyll occur earlier. Also the phytoplankton response at Papagayo is shorter, likely a result of the weaker nature of the Papagayo wind events.

[30] Figure 5 shows the composite maps of the natural logarithmic Chl-*a* concentration passing the 80% student t significance test on the day when surface Chl-*a* is highest. There are many fewer pixels for surface Chl-*a* that pass the significance test in comparison to SST (Figure 4), especially in the Gulf of Papagayo and Panama. This is primarily because there is a large amount of missing Chl-*a* data under the ITCZ cloud system, resulting in having Chl-*a* observations on average for only about 28% of all identified

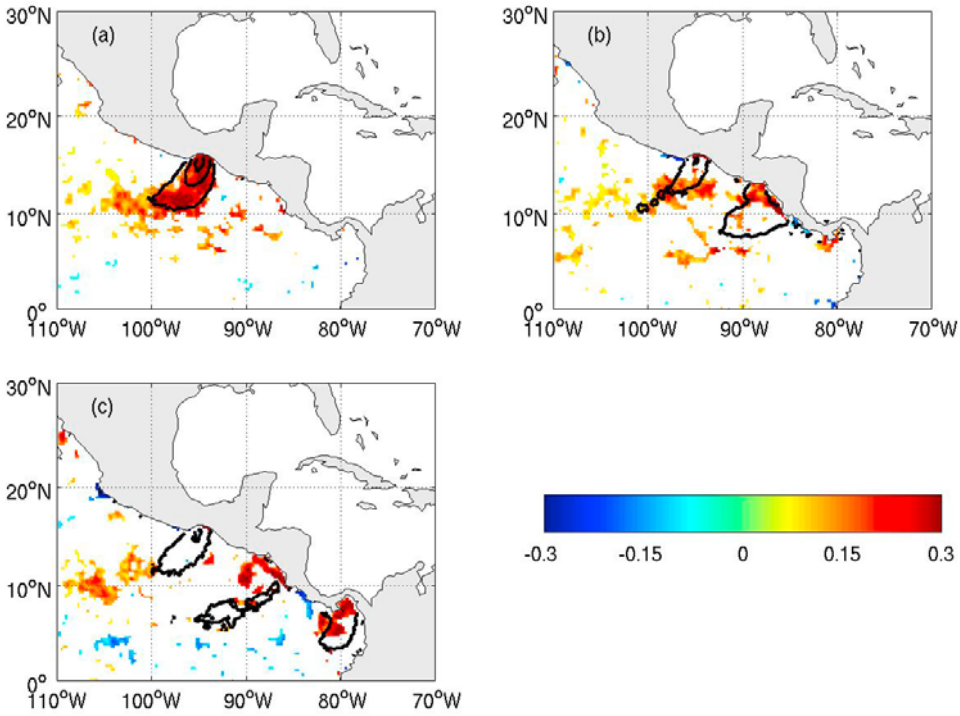

Figure 5. Composite maps of the high-frequency logarithmic chlorophyll-*a* anomaly (mg/m^3) passing 80% student *t* significance test for (a) Tehuantepec wind averaged over on day 0, (b) Papagayo wind averaged over day 1 and day 2, and (c) Panama wind averaged over day 1 and day 2. (Contours indicate wind speed of 4, 8, and 12 m/s.)

event days, while this fraction is approximately 73% for SST.

[31] Positive surface Chl-*a* signals for Tehuantepec and Panama winds occur right under the wind track and extend far into the ocean. The chlorophyll response for the Papagayo wind is intercepted by the Costa Rica Dome centered at 9°N, 90°W where the climatological surface Chl-*a* concentration and biological activity are typically higher than its surroundings [*Fiedler*, 2002]. In this region, the Chl-*a* concentration of subsurface water that would be brought up by wind-driven turbulent mixing is not distinctly higher than the surface Chl-*a* concentration within the dome region according to the WOA01 annual chlorophyll concentration data.

[32] Figure 6 displays the full time series of offshore wind velocity, SST and surface Chl-*a* in the gulf of Tehuantepec in 2005. We can see that the SST response is consistent with the picture we derived from the analysis of the composite high-frequency SST anomaly. SST plummets and soars back quickly. The lowest SST occurs between the day of maximum wind and two days after. The pattern of Chl-*a* response is, however, much more variable than that of the SST response. There are many factors influencing the rate of photosynthesis. Besides nutrient supplies and sunlight, other factors such as iron availability and sea water temperature also play a role in the rate of photosynthesis. Another factor that complicates our identification of the mean surface Chl-*a* response is the extended time scale of the Chl-*a* response to a wind event. The total time required for the initial increase due to mixing, the subsequent enhancement due to higher productivity and the final recovery is well beyond one week, while the separation interval we used to identify wind event is one week. If wind events are not well separated, the responses of different wind events will interfere with each other in our analysis.

[33] In order to assess the contribution of these wind events to net primary production (NPP), we inspect the composite time series of NPP in the three gulfs in Figures 3b, 3d, and 3f. Again, the confidence range is large due to the small size of the sample. Although the enhancement of Chl-*a* due to wind jets are similar in the three gulfs, inferred NPP is larger in the other two gulfs, possibly because there is more sunlight in lower latitudes. The maximum high-frequency NPP anomalies during wind events are 340, 358 and 383 mg C/(day m^2). The climatological NPP in the three gulfs is high and amounts to 1180, 1018 and 976 mg C/(day m^2), for the Gulfs of Tehuantepec, Papagayo and Panama, respectively. Thus, on average the typical wind event enhance daily NPP by about 30%, contributing substantially to the overall NPP of the region.

6. High-Frequency Gap Wind Events and Regional Mesoscale Variability

[34] It has been known that the eastern Pacific warm pool is a region of relatively high SSH variability, since satellite observations are available [*Willett et al.*, 2006]. These eddies transport biologically productive coastal waters into the interior ocean and possibly modulate the ecosystem of the pelagic waters along their paths [*Samuelsen and*

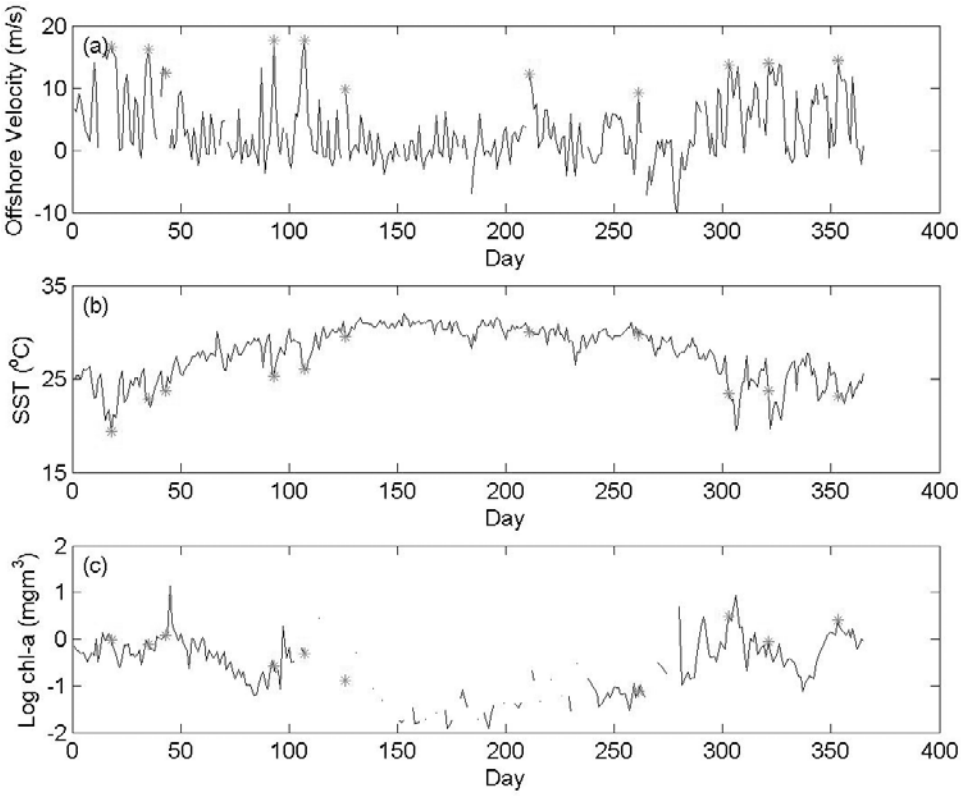

Figure 6. The time series of (a) offshore velocity (m/s) and (b) SST (°C). (c) Logarithmic surface chlorophyll-*a* concentration (mg/m^3) in the Gulf of Tehuantepec in 2005.

O'Brien, 2008]. Although the existence of high mesoscale variability is known, the generation mechanism of these eddies is still controversial. Some [e.g., *Giese et al.*, 1994] argued that the gap wind is the forcing mechanism for the regional SSH variability while others provided evidences supporting that barotropic and baroclinic instability triggered by poleward coastal Kelvin waves [*Zamudio et al.*, 2006] and the retroflection of the North Equatorial Counter Current (NECC) [*Hansen and Maul*, 1991] are responsible. In this section, we show that the statistical connection between high-frequency gap wind events and strong mesoscale eddies lends support to the first hypothesis put forward by *Giese et al.* [1994].

[35] Figures 7a and 7b show the maps of the standard deviation of high-frequency SSH anomaly in the eastern Pacific warm pool in boreal winter (January, February, and March) and in boreal summer (July, August, and September), respectively. The regional mesoscale variability exhibits strong seasonal variability as the wind events do. In boreal winter when there are more wind events, there are two narrow bands of high SSH variability emanating from the Gulfs of Tehuantepec and Papagayo, respectively. These two bands lie on the right flanks of the wind tracks where strong anticyclones are preferentially spun up by gap winds. The locations of the two bands suggest that the eddies have a direct or indirect connection with gap wind. The band from the Gulf of Tehuantepec extends to around 115°W 10°N, and the band from the Gulf of Papagayo extends to around 100°W 10°N. These two bands of high mesoscale activities are exceptionally narrow compared to the patterns of high mesoscale activities in major current systems like the Kuroshio and the Gulf Stream where current instabilities are the dominant mechanism for eddy generation. In boreal summer when there are few wind events, there is less mesoscale activity, and the patterns of high SSH variability are less organized. The narrowness, the location, and the seasonal variability of the high mesoscale activity bands all support the idea that the two bands of high mesoscale activities are largely associated with wind events as noted by *Giese et al.* [1994].

[36] Figure 7c displays the composite map high-frequency SSH anomaly passing the 95% student *t* test in the week following Tehuantepec wind events. Nearshore asymmetric circulations with a stronger anticyclone at the right flank of the wind track and weaker cyclone of at the left flank of the wind track are identified as a statistically significant signal. The nearshore asymmetric circulations were explored in detailed by *Trasviña et al.* [1995] and *McCreary et al.* [1989]. Hovmuller diagrams (Figures 7d and 7e) show that the strongest SSH signals originate from the two gulfs and propagate offshore. There are about twice as many positive large-amplitude SSH signals (>12 cm) than negative large-amplitude SSH signals (<−12 cm). It should be noted that eddies generated by current instabilities in other current systems (e.g., the California Current System) do not have a preference for eddy polarity [*Chelton et al.*, 2007]. In contrast, wind jets tend to preferentially spin up anticyclonic eddies (positive SSH anomaly) in this region [*McCreary et al.*, 1989]. There are some SSH signals that do not emanate from the coast. These high-frequency SSH signals are weaker than those from the coast and are likely caused by the barotropic and baroclinic instability of currents [*Farrar*

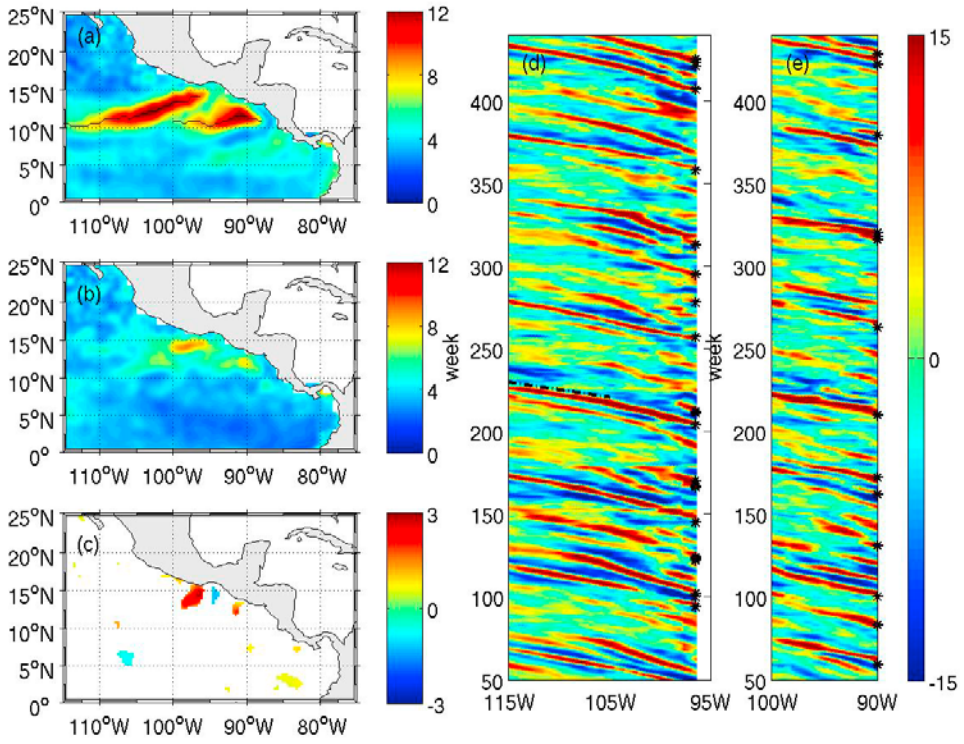

Figure 7. Standard deviation of high-frequency SSH anomaly (cm) in (a) January, February, and March and (b) July, August, and September. (c) Composite map of high-frequency SSH anomaly passing 95% student *t* significance test on the week after Tehuantepec wind events. Hovmuller diagram for SSH anomaly originating from (d) the Gulf of Tehuantepec and (e) the Gulf of Papagayo. The black line in Figure 7a indicates the positions from which the Hovmuller diagrams are sampled. The black dash line in Figure 7d indicates eddies with an approximate speed of 15 cm/s. Asterisks in Figures 7d and 7e denote identified wind events that precede a strong eddy.

and Weller, 2006]. Tehuantepec eddies propagate southwestward after leaving the coast and turn westward at around 105°N while Papagayo eddies propagate westwards. The propagation speed for an eddy is estimated by dividing the distance by the time the eddy has travelled. The averaged propagation speed is approximate 15 ± 3 cm/s (Figure 7d), close to the phase speed of linear nondispersive first-mode baroclinic Rossby waves at the same latitude [*Chelton and Schlax*, 1996]. The variability of the eddy propagation speeds is likely the result of variable background mean currents and variable stratification.

[37] The wind events that were followed by strong anticyclones within less than two weeks are indicated by asterisks in the Hovmuller diagram (the time resolution of the SSH maps precludes a more detailed time relationship). There are fifteen strong anticyclonic eddies emanating from the Gulf of Tehuantepec with SSH anomalies larger than 12 cm, and thirteen of them were preceded by a Tehuantepec wind event within less than two weeks. Of the remaining two eddies, one was preceded by persistent offshore strong wind that lasted for about a week and was excluded by the our event detection criterion given its unusual duration; the other one was not associated with any strong offshore wind and was therefore likely due to current instabilities. Five other eddies originated from east of the 94°W and passed the Gulf of Tehuantepec. Those were likely generated by current instabilities possibly triggered by coastal Kelvin waves [*Zamudio et al.*, 2006]. For the Gulf of Papagayo, we identified eighteen anticyclonic eddies whose SSH anomaly exceeded 12 cm. Thirteen of them were preceded by Papagayo wind events by less than two weeks. Three other eddies were preceded by strong wind events that lasted longer than typical and were excluded by our event detection criterion. The two other eddies were observed in fall when the NECC reaches the coast of central America [*Kessler*, 2006]. They were thus possibly due to the retroflection of the NECC [*Hansen and Maul*, 1991] and current instabilities. In summary, the vast majority of the strong eddies emanating from the two gulfs were preceded by high wind event. This corroborates the notion that transient wind forcing is the primary mechanism forcing mesoscale eddies in this regions.

7. Conclusions

[38] Based on 8 year satellite and reanalysis data sets, the physical and biological responses of the northeastern tropical Pacific to the intense and intermittent wind jets through three mountain gaps in Central America are characterized through multivariate statistical composites. This extends and largely confirms previous individual case studies for this region, suggesting that the long-term average response to such wind events follows relatively predictable patterns in all three Gulf regions. Strong wind-driven turbulence entrains subsurface waters of lower temperature, higher phytoplankton biomass concentration, and richer

nutrients to the ocean surface. Wind-driven shear turbulent mixing is responsible for the dominant SST and surface Chl-*a* signals. The positive heat flux anomaly from the atmosphere to the ocean associated with the negative SST disturbance dominates other horizontal and vertical processes in the sea surface warming after wind events. Ocean productivity is considerably enhanced during and after wind events, this is reflected in the time series of surface Chl-*a*. In the three gulf regions of the northeastern tropical Pacific, the high-frequency gap wind events contribute as high as 29% to 39% to daily NPP. Satellite SSH anomaly data reveal that the high-frequency gap wind events play a role in the generation of high-frequency mesoscale in the northeastern tropical Pacific and have a wide-reaching effect on the ocean in the form of westward propagating eddies. This typical response substantially extends the results gained from individual case studies, as it permits to make the conclusions more general, and applicable also to other gap wind systems.

[39] The insights gained in our analyses for the Central American gap winds can help to understand better the oceanic impact of gap winds in other regions of the world. Narrow wind jets can be found in several places, especially where the orography near the coast drops suddenly. Well-known examples include gap winds in Southern California induced by Santa Ana wind conditions [e.g., *Hu and Liu*, 2003; *Trasviña et al.*, 2003b], the Greenland tip jet off the southern tip of Greenland [e.g., *Pickart et al.*, 2003], and the Mistral over the Gulf of Lion [e.g., *Hong et al.*, 2007]. Similar to the Central American gap winds, the Santa Ana wind also created cold filaments and enhanced surface Chl-*a* [*Hu and Liu*, 2003; *Trasviña et al.*, 2003b]. In contrast, no chlorophyll enhancement has been reported downwind of the Greenland tip jet, primarily because this wind induces such deep convection that light becomes limiting for phytoplankton. In fact, the sea surface cooling due to Greenland tip jet is so strong that the induced convection, which deepens the mixed layer to 2000 meters, is a possible mechanism for deep water formation in the Irminger Sea in winter [*Pickart et al.*, 2003]. *Pickart et al.* [2003] also observed cyclonic circulation spun up by the strong wind curl at the left flank of the wind track. *Hong et al.* [2007] reported the importance of the Mistral on the deep convection in the Gulf of Lion. Although wind jets all over the world differ in strength, spatial scale and duration, we expect that boundary layer turbulence enhances under the wind tracks due to mechanical and/or thermal forcing and recirculations are spun up by strong wind curls at the two flanks of the wind tracks. Local hydrography and background circulations modulate the oceanic responses. SST decreases when strong turbulence entrains cold water from beneath the mixed layer. Surface Chl-*a* increases and productivity enhances in the low and middle latitude where the DCM is found and the productivity is mainly nutrient limited.

[40] Despite our progress, there are still a few outstanding research questions regarding the oceanic responses of gap winds and their mechanisms. For example, how quantitatively important are the transient wind forcing and current instabilities for the generation of the regional mesoscale eddies? What determines the narrow paths of eddies out of the Gulfs of Tehuantepec and Papagayo? How important are the high-frequency wind events in the seasonal cycle of surface Chl-*a*? How does the transport of carbon and nutrients by eddies modulate the regional carbon-nitrogen-phosphorus dynamics? The authors are currently trying to address these questions by a regional ocean modeling study, which is able to provide insights into detailed physical and biological processes.

[41] **Acknowledgments.** The authors wish to thank Dudley Chelton for sharing the eddy tracking results in the northeastern tropical Pacific, and Xiao Han for doing some of the initial analyses for this project. Comments from Des Barton and two anonymous reviewer greatly contributed to the improvement this manuscript. This work is supported by NASA headquarters under the Earth System Science Fellowship grant NNX08AU98H. N.G. acknowledges support from ETH Zurich.

References

Barton, E. D., M. L. Argote, J. Brown, P. M. Kosro, M. Lavín, J. M. Robles, R. L. Smith, A. Trasviña, and H. S. Velez (1993), Supersquirt: Dynamics of the Gulf of Tehuantepec, Mexico, *Oceanography*, *6*, 23–30.

Barton, E. D., M. Lavín, and A. Trasviña (2009), Coastal circulation and hydrography in the Gulf of Tehuantepec, Mexico, during winter, *Continental Shelf Res.*, *29*, 23–30.

Behrenfeld, M. J., and P. G. Falkowski (1997), Photosynthetic rates derived from satellite-based chlorophyll concentration, *Limnol. Oceanogr.*, *42*(1), 1–20.

Bretherton, F. P. (1982), Ocean climate modeling, *Prog. Oceanogr.*, *11*, 93–129.

Campbell, J. W. (1995), The lognormal distribution as a model for bio-optical variability in the sea, *J. Geophys. Res.*, *100*(C7), 13,237–13,254.

Chelton, D. B., and M. G. Schlax (1996), Global observations of oceanic Rossby waves, *Science*, *272*, 234–238.

Chelton, D. B., M. H. Freilich, and S. K. Esbensen (2000a), Satellite observations of the wind jets off the Pacific Coast of Central America. Part I: Case studies and statistical characteristics, *Mon. Weather Rev.*, *128*, 1993–2018.

Chelton, D. B., M. H. Freilich, and S. K. Esbensen (2000b), Satellite observations of the wind jets off the Pacific coast of Central America. Part II: Regional relationships and dynamical considerations, *Mon. Weather Rev.*, *128*, 2019–2043.

Chelton, D. B., M. G. Schlax, M. H. Freilich, and R. F. Milliff (2004), Satellite measurements reveal persistent small-scale features in ocean winds, *Science*, *303*, 978–983, doi:10.1126/science.1091901.

Chelton, D. B., M. G. Schlax, R. M. Samelson, and R. A. de Szoeke (2007), Global observations of large oceanic eddies, *Geophys. Res. Lett.*, *34*, L15606, doi:10.1029/2007GL030812.

Clarke, A. J. (1988), Inertial wind path and sea surface temperature patterns near the Gulf of Tehuantepec and Gulf of Papagayo, *J. Geophys. Res.*, *93*, 15,491–15,501.

Conkright, M. E., R. A. Locarnini, H. E. Garcia, T. D. O'Brien, T. P. Boyer, C. Stephens, and J. I. Antonov (2002), World ocean atlas 2001: Objective analyses, data statistics, and figures [CD-ROM], *Natl. Oceanogr. Data Cent. Internal Rep. 17*, 17 pp., Ocean Clim. Lab., Silver Spring, Md.

Crepon, M., and C. Richez (1982), Transient upwelling generated by two-dimensional atmospheric forcing and variability in the coastline, *J. Phys. Oceanogr.*, *12*, 1437–1456.

Giese, B. S., J. A. Carton, and L. J. Holl (1994), Sea level variability in the eastern tropical Pacific as observed by TOPEX and Tropical Ocean-Global Atmosphere Tropical Atmosphere-Ocean Experiment, *J. Geophys. Res.*, *99*(C12), 24,739–24,748.

Farrar, J. T., and R. A. Weller (2006), Intraseasonal variability near 10°N in the eastern tropical Pacific Ocean, *J. Geophys. Res.*, *111*, C05015, doi:10.1029/2005JC002989.

Fiedler, P. C. (2002), The annual cycle and biological effects of the Costa Rica Dome, *Deep Sea Res. Part A*, *49*, 321–338.

Frankenfield, H. C. (1917), "Northers" of the Canal Zone, *Mon. Weather Rev.*, *45*, 546–550.

Hansen, D. V., and G. A. Maul (1991), Anticyclonic current rings in the eastern Pacific Ocean, *J. Geophy. Res.*, *96*(C4), 192–194.

Hong, X., R. M. Hodur, and P. J. Martin (2007), Numerical simulation of deep-water convection in the Gulf of Lion, *Pure Appl. Geophys.*, *164*, 2101–2116.

Hu, H., and W. T. Liu (2003), Oceanic thermal and biological responses to Santa Ana winds, *Geophys. Res. Lett.*, *30*(11), 1596, doi:10.1029/2003GL017208.

Hurd, W. E. (1929), Northers of the Gulf of Tehuantepec, *Mon. Weather Rev.*, *57*, 6965–6979.

Kanamitsu, M., W. Ebisuzaki, J. Woollen, S.-K. Yang, J. J. Hnilo, M. Fiorino, and G. L. Potter (2002), NCEP-DEO AMIP-II reanalysis (R-2), *Bull. Am. Meteorol. Soc.*, *83*, 1631–1643.

Kessler, W. S. (2006), The circulation of the eastern tropical Pacific: A review, *Prog. Oceanogr.*, *69*, 181–217, doi:10.1016/j.pocean.2006.03.009.

McClain, C. R., J. R. Christian, S. R. Signorini, M. R. Lewis, I. Asanuma, D. Turk, and C. Dupouy-Douchement (2002), Satellite ocean-color observations of the tropical Pacific Ocean, *Deep Sea Res. Part II*, *49*, 2533–2560.

McCreary, J. P., Jr., H. S. Lee, and D. B. Enfield (1989), The response of the coastal ocean to strong offshore winds: With application to the Gulfs of Tehuantepec and Papagayo, *J. Mar. Res.*, *47*, 81–109.

Palacios, D. M., and S. J. Bograd (2005), A census of Tehuantepec and Papagayo eddies in the northeastern tropical Pacific, *Geophys. Res. Lett.*, *32*, L23606, doi:10.1029/2005GL024324.

Pascual, A., Y. Faugère, G. Larnicol, and P.-Y. Le Traon (2006), Improved description of the ocean mesoscale variability by combining four satellite altimeters, *Geophys. Res. Lett.*, *33*, L02611, doi:10.1029/2005GL024633.

Pickart, R. S., M. A. Spall, M. H. Ribergaard, G. W. K. Moore, and R. F. Milliff (2003), Deep convection in the Irminger Sea forced by the Greenland tip jet, *Nature*, *424*, 152–156, doi:10.1038/nature01729.

Price, J. F., R. A. Weller, and R. Pinkel (1986), Diurnal cycling: Observations and models of the upper ocean response to diurnal heating, cooling, and wind mixing, *J. Geophys. Res.*, *91*(C7), 8411–8427.

Price, J. F., J. Morzel, and P. P. Niiler (2008), Warming of SST in the cool wake of a moving hurricane, *J. Geophys. Res.*, *113*, C07010, doi:10.1029/2007JC004393.

Rodríguez-Rubio, E., W. Schneider, and R. Abarca del Río (2003), On the seasonal circulation within the Panama Bight derived from satellite observations of wind, altimetry and sea surface temperature, *Geophys. Res. Lett.*, *30*(7), 1410, doi:10.1029/2002GL016794.

Romero-Centeno, R., J. Zavala-Hidalgo, A. Gallegos, and J. J. O'Brien (2003), Tehuantepec isthmus wind climatology and ENSO signal, *J. Clim.*, *16*, 2628–2639.

Rossow, W. B., and R. A. Schiffer (1991), ISCCP cloud data products, *Bull. Am. Meteorol. Soc.*, *71*, 2–20.

Samuelsen, A., and J. J. O'Brien (2008), Wind-induced cross-shelf flux of water masses and organic matter at the Gulf of Tehuantepec, *Deep Sea Res. Part I*, *55*, 221–246, doi:10.1016/j.dsr.2007.11.007.

Steenburgh, W. J., D. M. Schultz, and B. A. Colle (1998), The structure and evolution of gap outflow over the Gulf of Tehuantepec, Mexico, *Mon. Weather Rev.*, *126*, 2673–2691.

Sun, F., and J.-Y. Yu (2006), Impacts of Central America gap winds on the SST annual cycle in the eastern Pacific warm pool, *Geophys. Res. Lett.*, *33*, L06710, doi:10.1029/2005GL024700.

Trasviña, A., and E. D. Barton (2008), Summer circulation in the Mexican tropical Pacific, *Deep Sea Res. Part I*, *55*, 587–607.

Trasviña, A., E. D. Barton, J. Brown, H. S. Vélez, P. M. Kosro, and R. L. Smith (1995), Offshore wind forcing in the Gulf of Tehuantepec, Mexico: The asymmetric circulation, *J. Geophys. Res.*, *100*, 20,649–20,663.

Trasviña, A., E. D. Barton, H. S. Vélez, and J. Brown (2003a), Frontal subduction of a cool surface water mass in the Gulf of Tehuantepec, Mexico, *Geofis. Int.*, *42*(1), 101–114.

Trasviña, A., M. Ortiz-Figueroa, H. Herrera, and M. A. Cosío (2003b), 'Santa Ana' winds and upwelling filaments off northern Baja California, *Dyn. Atmos. Oceans*, *37*, 113–129.

Wang, C. (2007), Variability of the Caribbean low-level jet and its relations to climate, *Clim. Dyn.*, *29*, 411–422.

Wentz, F. J., C. Gentemann, D. Smith, and D. Chelton (2000), Satellite measurements of sea surface temperature through clouds, *Science*, *288*, 847–850, doi:10.1126/science.288.5467.847.

Willett, C. S., R. R. Leben, and M. F. Lavín (2006), Eddies and tropical instability waves in the eastern tropical Pacific: A review, *Prog. Oceanogr.*, *69*, 218–238, doi:10.1016/j.pocean.2006.03.010.

Xie, S. P., H. Xu, W. S. Kessler, and M. Nonaka (2005), Air-sea interaction over the eastern Pacific warm pool: Gap winds, thermocline dome, and atmospheric convection, *J. Clim.*, *18*(1), 5–20.

Yu, L., and R. A. Weller (2007), Objectively analyzed air-sea heat fluxes for the global oce-free oceans (1981–2005), *Bull. Am. Meteorol. Soc.*, *88*, 527–539.

Zamudio, L., H. E. Hurlburt, E. J. Metzger, S. L. Morey, J. J. O'Brien, C. E. Tilburg, and J. Zavala-Hidalgo (2006), Interannual variability of Tehuantepec eddies, *J. Geophys. Res.*, *111*, C05001, doi:10.1029/2005JC003182.

N. Gruber, Institute of Biogeochemistry and Pollutant Dynamics, ETH Zurich, Building CHN, Office E31.2, Universitatstrasse 16, CH-8092 Zurich, Switzerland.

J.-H. Liang, Department of Atmospheric and Oceanic Sciences, University of California, Mathematical Sciences Building, Room 7127, Los Angeles, CA 90095-1565, USA. (liangjh@atmos.ucla.edu)

J. C. McWilliams, Department of Atmospheric and Oceanic Sciences, University of California, Mathematical Sciences Building, Room 7983, Los Angeles, CA 90095-1565, USA.